J. Fluid Mech. (1997), *vol.* 347, *pp.* 171–195. Printed in the United Kingdom

An analysis of rotating shear flow using linear theory and DNS and LES results

By A. SALHI[1] AND C. CAMBON[2]

[1]Département de Physique, Faculté des Sciences de Tunis, 1060, Tunis, Tunisia

[2] Ecole Centrale de Lyon/Université Claude Bernard - Lyon, Laboratoire de Mécanique des Fluides et d'Acoustique, UMR 5509, BP 163, 69131 Ecully Cedex, France.

(Received 14 July 1995 and in revised form 6 May 1997)

The development of turbulence is investigated in the presence of a mean plane shear flow (rate S) rotating with angular velocity vector (rate Ω) perpendicular to its plane. An important motivation was generalizing the work by Lee, Kim & Moin (1990) to rotating shear flow, in particular detailed comparisons of homogeneous rapid distortion theory (RDT) results and the databases of homogeneous and channel flow direct numerical simulations (DNS). Linear analysis and related RDT are used starting from the linearized equations governing the fluctuating velocity field. The parameterization based on the value of the Bradshaw–Richardson number $B = R(1 + R)$ (with $R = -2\Omega/S$) is checked against complete linear solutions. Owing to the pressure fluctuation, the dynamics is not governed entirely by the parameter B, and the subsequent breaking of symmetry (between the R and $-1 - R$ cases) is investigated. New analytical solutions for the 'two-dimensional energy components' $\mathscr{E}_{ij}^{(l)} = E_{ij}(k_l = 0, t)$ (i.e. the limits at $k_l = 0$ of the one-dimensional energy spectra) are calculated by inviscid and viscous RDT, for various ratios Ω/S and both streamwise $l = 1$ and spanwise $l = 3$ directions. Structure effects (streak-like tendencies, dimensionality) in rotating shear flow are discussed through these quantities and more conventional second-order statistics. In order to compare in a quantitative way RDT solutions for single-point statistics with available large-eddy simulation (LES) data (Bardina, Ferziger & Reynolds 1983), an 'effective viscosity' model (following Townsend) is used, yielding an impressive agreement.

1. Introduction

Rotating turbulent flows occur in fields as diverse as engineering (e.g. turbomachinery, combustion engines with swirl and tumble), geophysics and astrophysics. Studies of such flows have shown complex coupling between Coriolis forces, pressure and strain. Effects of curvature and advection by large eddies can often be considered as similar to those of rotation and analysed in the same way. Combined effects of strain and background rotation are present in many actual flow configurations. The case of the pure plane shear flow in a rotating frame is of particular interest, and was studied both experimentally (Johnston, Hallen & Lezius 1972) and numerically (see Kristoffersen & Andersson 1993, for a recent and comprehensive direct numerical simulation, DNS, study). The basic case of shear with constant rate S, in a frame rotating with constant angular velocity Ω, is shown in figure 1. Simple analyses were also proposed to predict the ranges of stabilization and destabilization, with

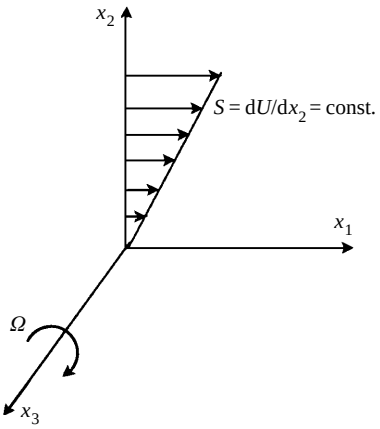

FIGURE 1. Homogeneous turbulent shear flow in a rotating frame.

unexpected success. Among them, the Bradshaw criterion (Bradshaw 1969), recalled below, is the most popular. On the grounds of an analogy between rotation curvature and density stratification, Bradshaw (1969) defined an equivalent *gradient Richardson number* as

$$B = 2\Omega(2\Omega - S)/S^2 = R(1 + R)$$

in order to identify the stability of a rotating unidirectional shear flow (where the rotation axis is perpendicular to the plane of the mean flow.) The rotation number $R = -2\Omega/S$ is chosen here as the ratio of system vorticity 2Ω to shear-induced vorticity $-S$. According to the value and the sign of the B-parameter (called the Bradshaw–Richardson number hereinafter) there are three different cases: the neutral case when $B = 0$ (which includes both the pure shear flow, $\Omega = 0$, and the 'zero absolute vorticity' flow, $2\Omega - S = 0$), the unstable case when $B < 0$ and the stable case when $B > 0$. Even if the stability is satisfactorily predicted by the Bradshaw analogy, the symmetry between R and $-1 - R$, assumed by using the Bradshaw–Richardson number as the unique parameter for linear development, is not confirmed by the results. This weakness in the Bradshaw approach is easily understood since the analysis ultimately can be recovered from an oversimplified linear analysis, which is *pressureless* (see Speziale & Mac Giolla Mhuiris 1989*a*, and Cambon *et al.* 1994, for a detailed discussion). Three-dimensional linear stability analyses, capable of taking into account the pressure perturbation, confirmed the value $R = -1/2$ for maximum destabilization but exhibited an important asymmetry with respect to $R = -1/2$. For example the case of zero rotation (pure shear, $R = 0$) was found to be very different from the case of zero absolute vorticity $R = -1$, even if both cases were considered as neutral in the Bradshaw approach.

Looking at the non-rotating case, the work of Lee, Kim & Moin (1990) showed the unexpected agreement between homogeneous rapid distortion theory (RDT) with constant shear rate and DNS results in a channel flow at high shear rate. Even the tendency to develop *streak-like* structures can be obtained in pure inviscid homogeneous RDT when looking at the time history of some 'two-dimensional energy components' (or products of integral length scales and related Reynolds stress components, Cambon 1990). The most interesting laws, given by inviscid RDT, were $\langle u_1^2\rangle L_{11}^1 \propto 1 + (St)^2/2$ and $\langle u_1^2\rangle L_{11}^3 =$ Constant (Cambon 1990), where L_{11}^1 is the streamwise integral length scale (related to the length of the streak-like structure)

and L_{11}^3 is the spanwise one (related to the spacing of the streak-like structure). The physical relevance of such combinations of Reynolds stresses and integral length scales was shown in the analysis of pure rotation effects (Jacquin *et al.* 1990), and their interpretation as *two-dimensional energy components* justified. In addition, simple analytical RDT solutions can be found for these quantities, but not for the Reynolds stresses or the integral length scales considered separately.

In order to investigate the role of pressure and the alteration of structure and statistics due to system rotation, an improved version of RDT is extensively used, following the method and the formalism of Cambon (1982) (updated in Cambon *et al.* 1994), which do not essentially differ from those of Townsend (1976). The starting point is solving linearized equations that govern the fluctuating velocity field for arbitrary initial data, rather than solving the linear contribution to an equation (often referred to as the Craya equation, Craya 1958) for *statistical second-order moments*; (see Deissler 1970, Courseau & Loiseau 1978; Bertoglio 1982, for the latter approach). In addition to inviscid and viscous RDT, some corrections proposed by Townsend (1970), RDT corrected for decay, (hereafter referred to as RDTT) will be compared to available RDT and DNS results, following preliminary applications by Salhi (1993).

The paper is organized as follows. The background for the linear analysis of the fluctuating field, in the presence of the rotating shear, is presented in §2, and subsequent RDT for second-order statistics is introduced. An analytical derivation of two-dimensional energy components with both spanwise and streamwise separations is performed in §3. Comparisons between LES (Bardina, Ferziger & Reynolds 1983) and RDTT (Townsend approach) are given in §4. The qualitative RDT results are discussed in §5, in connection with some actual structural features identified in a rotating channel flow. Finally §6 contains a discussion of the main results and conclusions.

2. Linear analysis

2.1. *The role of the pressure in the presence of rotation*

As recalled and discussed in §1, the most popular criterion for the stability of rotating shear flow (figure 1) is based on the sign of the Bradshaw–Richardson number $B = R(R+1)$ where $R = -2\Omega/S$ is the rotation number, which is defined in this paper as the ratio of system vorticity (2Ω) and shear-induced vorticity ($-S$). This criterion can be introduced using different approaches, but it ultimately comes from a simplified *pressure-less* linear analysis, which is also two-component regarding the fluctuating velocity field (only the components in the plane of the mean shear are needed). The 'pressureless' aspect is either explicit or implicit (implicit as in the 'displaced particle approach', Tritton 1981), and it is possible to look either at the equations for the fluctuating velocity field u_i (Speziale & Mac Giolla Mhuiris 1989*a*), or at the equations for the Reynolds stress tensor $\langle u_i u_j \rangle$ (Tritton 1992).

All approaches can be started from the following linearized equations for velocity u_i and pressure p disturbances in the presence of mean shear and Coriolis force:

$$\dot{u}_i = -S \underbrace{(\delta_{i1}\delta_{j2} + 2(\Omega/S)\epsilon_{i3j})}_{M_{ij}} u_j + (1/\rho_0)\partial p/\partial x_i + \nu \nabla^2 u_i, \tag{1}$$

in which $\dot{u}_i = \partial u_i/\partial t + S x_2 \partial u_i/\partial x_1$ denotes the substantial derivative along the mean flow, ϵ_{ijk} is the third-order alternating tensor, ν is the kinematic viscosity, and ρ_0 is the density. The first two terms in the right-hand side involve the matrix M_{ij}

whose non-zero eigenvalues are $\pm(-B)^{1/2}$. Hence the amplification of $\boldsymbol{u}$ (which only concerns the two components u_1, u_2) is governed by $\exp(\pm(-B)^{1/2}St)$ when solving the simplified initial value problem (1) in the absence of pressure (and viscous) effect. Consequently a simple parameterization in terms of St and B is found.

The role of the fluctuating pressure, in connection with the incompressibility constraint $u_{i,i} = 0$, is accounted for in a true three-dimensional linear stability analysis, or in homogeneous RDT, solving the complete equation (1) for arbitrary initial data. The results seem not to question the fact that the case $R = -1/2$ (minimal negative value $-1/4$ for B), is the most destabilizing one. The pressure is responsible, however, for the loss of symmetry shown when comparing the cases R and $-1 - R$ (such a symmetry holds provided that B is assumed to be the only relevant parameter). Of special interest to this loss of symmetry are the two presumed neutral cases ($R = 0$ and $R = -1$), which correspond to the same value $B = 0$: the non-rotating case $R = 0$ is characterized by a complicated inviscid linear solution (RDT, Townsend), which gives more amplification than the case of zero absolute vorticity $R = -1$, whose related linear solution can be easily derived from a Cauchy solution for the fluctuating vorticity field (Cambon *et al.* 1994). On the other hand, it is noteworthy that when turbulence is initially two-dimensional (in the plane of the mean flow) the velocity fluctuation is unaffected by system rotation (only the pressure fluctuation is affected by both shear and rotation).

In short, a simplified analysis using a pressureless *two-component* perturbation velocity field is partially relevant to predict the range of stabilization–destabilization in a rotating shear flow, whereas an analysis using a two-dimensional perturbation field including the pressure is not. This is explained by the essential role of pure spanwise modes in the complete linear stability problem (Cambon *et al.* 1994; Leblanc & Cambon 1997).

From the standpoint of single-point modelling, which is outside the scope of the present paper, the issues discussed above are of great interest. Let us recall that a k–ε model is basically insensitive to system rotation, so that only an '*ad hoc*' correction of the 'production' terms, including Richardson-dependent scalar coefficients, is possible. Full Reynolds stress models can take into account stabilizing-destabilizing effects through the 'production-Coriolis redistribution' tensor $S(M_{il}\langle u_l u_j\rangle + M_{jl}\langle u_i u_l\rangle)$ ($\boldsymbol{M}$ as in (1)), which reflects pressureless parameterization, whereas effects of fluctuating pressure are reflected in the 'rapid' pressure–strain correlation tensor. Present models for pressure–strain correlations yield an asymmetry (different development for R and for $-1 - R$), but the maximum amplification of turbulence is found for values significantly different from $R = -1/2$ (see Speziale & Mac Giolla Mhuiris 1989*a*, *b*.)

2.2. *Complete linear analysis*

Since the velocity field is unbounded (no boundary conditions), in agreement with statistical homogeneity, Fourier transformation, which is an invaluable tool for treating pressure effects, is used to seek solenoidal ($u_{i,i} = 0$) solutions of the linearized equation (1)

$$(.)(\boldsymbol{x}, t) = \int \exp(\mathrm{i}\boldsymbol{x}\cdot\boldsymbol{k})\hat{(.)}(\boldsymbol{k}, t)\mathrm{d}^3\boldsymbol{k},$$

where $\mathrm{i}^2 = -1$. Here $\boldsymbol{k} = (k_1, k_2, k_3)$ is the wave vector, which is considered as time-dependent in order to follow the advection by the mean, and its initial (at $t = 0$) value is denoted $\boldsymbol{K} = (K_1, K_2, K_3)$, so that

$$k_1 = K_1 = K\cos\varphi\sin\theta, \tag{2a}$$

$$k_2 = K_2 - K_1 St = K \sin\theta(\sin\varphi - St\cos\varphi), \tag{2b}$$

$$k_3 = K_3 = K\cos\theta \tag{2c}$$

(Townsend 1976) where (K, θ, φ) is a spherical coordinates system for $\boldsymbol{K}$. Eliminating the pressure from (1) in Fourier space by means of the incompressibility condition, we obtain the equation for the Fourier transform of the velocity fluctuation

$$\dot{\hat{u}}_i + \frac{\nu k^2}{S}\hat{u}_i = -\underbrace{\left[\left(\delta_{i1}\delta_{j2} + 2\frac{\Omega}{S}\epsilon_{i3j}\right) - \frac{k_i k_n}{k^2}\left(2\delta_{n1}\delta_{j2} + 2\frac{\Omega}{S}\epsilon_{n3j}\right)\right]}_{\mathscr{L}_{ij}}\hat{u}_j \tag{3}$$

where the overdot denotes the time derivative at fixed $\boldsymbol{K}$, in terms of the dimensionless parameter St. Of course, the contribution of M_{ij} in (1) is recovered as the first term in $\mathscr{L}_{ij}$, whereas the additional (k_i/k-dependent) term corresponds to the explicit contribution from the fluctuating pressure. The solution can be written as

$$\hat{u}_i(\boldsymbol{k}, t) = \exp\left(-\frac{\nu k^2}{S} f(\boldsymbol{k}/k, St)\right) G_{ij}(\boldsymbol{k}/k, t)\hat{u}_j(\boldsymbol{K}, t = 0), \tag{4}$$

where

$$f(\boldsymbol{k}/k, St) = St\left(1 + \frac{k_1 k_2}{k^2}St + \frac{k_1^2}{k^2}\frac{(St)^2}{3}\right) \tag{5}$$

is involved in the viscous term, calculated as an integrating factor.

As a last simplification, the velocity intensity $\hat{u}_i$ is sought in terms of two components $\hat{\phi}^\alpha = \hat{u}_i e_i^\alpha, \alpha = 1, 2$ in the plane normal to $\boldsymbol{k}$ (due to the incompressibility constraint), so that the rank-three matrix $\boldsymbol{G}$ can be replaced by a rank-two matrix $\boldsymbol{g}$ for generating the complete linear solution similar to (4) (see Cambon 1982; Cambon *et al.* 1994, and Appendix A for details). Even if the linear stability, or linear dynamics, is governed by the *deterministic* matrix $\boldsymbol{g}$ only in the inviscid case, and by both $\boldsymbol{g}$ and f in the viscous case, complete RDT solutions for second-order *statistics* are also of interest, and are considered in the following.

2.3. *RDT for second-order statistics*

All second-order statistics, including single and two-point velocity (and also vorticity and 'rapid' pressure, and so on) correlations, can be derived from the second-order spectral tensor $\Phi_{ij}(k_1, k_2, k_3, t)$. This tensor, which is the Fourier transform of the velocity correlations at two points, is defined in *homogeneous turbulence* by

$$\langle \hat{u}_i^*(\boldsymbol{p}, t)\hat{u}_j(\boldsymbol{k}, t)\rangle = \Phi_{ij}(\boldsymbol{k}, t)\delta(\boldsymbol{p} - \boldsymbol{k}).$$

Using the previous linear relationship for $\hat{\boldsymbol{u}}$ (4), Φ_{ij} can be calculated (with arbitrary initial values) as

$$\Phi_{ij}(\boldsymbol{k}, t) = \exp(-2\nu k^2 f/S) G_{il} G_{jn} \Phi_{ln}(\boldsymbol{K}, t = 0).$$

Assuming that the turbulence is initially isotropic, the spectral tensor is found as follows, as the product of three contributions, namely Φ_{ij}^g which reflects the *deterministic* and inviscid linear mechanismes, the *statistical* initial data, and the viscous term:

$$\Phi_{ij}(\boldsymbol{k}, t) = \Phi_{ij}^g(\boldsymbol{k}/k, t)\frac{E(K, 0)}{4\pi K^2}\exp\left(-2\frac{\nu k^2}{S}f(\boldsymbol{k}/k, t)\right). \tag{6}$$

The deterministic factor Φ^g only involves the matrix $\boldsymbol{G}$ (equation (4)); its expression is facilitated using the $\boldsymbol{g}$ matrix and the (e, Z) decomposition of the spectral tensor

(Cambon & Jacquin 1989), so that

$$\Phi_{ij}^g = e^g P_{ij} + \mathrm{Re}(Z^g N_i N_j), \tag{7}$$

with

$$P_{ij} = \delta_{ij} - k_i k_j / k^2, \qquad \boldsymbol{N} = \boldsymbol{e}^{(2)} - \mathrm{i}\boldsymbol{e}^{(1)},$$

$$e^g = g_{\alpha\beta} g_{\alpha\beta}/2, \qquad Z^g = (g_{2\alpha} g_{2\alpha} - g_{1\alpha} g_{1\alpha})/2 + \mathrm{i}(g_{11} g_{21} + g_{22} g_{12}).$$

From (6) it is clear that the RDT solution involves both orientation and modulus of the wavevector, but only the initial data and the viscous factor display the dependency with respect to the modulus (or *size* of the structures). Accordingly, the *inviscid* RDT history of any single-point correlation, that is obtained by integration over wave-space (in terms of K, θ, ϕ in (2)), is independent of the form of $E(K,0)$ since the contribution of initial data amounts to, e.g. the initial kinetic energy $q_0^2/2 = \int_0^\infty E(K,0)\mathrm{d}K$ only. On the other hand, the viscous factor in (6) affects the RDT history in a way which depends on the shape of $E(K,0)$. Hence a model for $E(K,0)$ has to be specified for viscous applications, and especially for introducing a correction for decay in agreement with Townsend's (1976) proposal.

For this purpose we consider the following form (Townsend 1976; Hunt & Carruthers 1990) that decreases very rapidly with increasing wavenumber:

$$E(K,0) \propto K^N \exp(-K^2 L^2/2), \tag{8}$$

where N is integer ($N \geqslant 0$) and L is a measure of the size of the largest eddies, or an integral scale. Equation (6) becomes

$$\Phi_{ij}(\boldsymbol{k},t) = \Phi_{ij}^g(\boldsymbol{k}/k,t) K^{N-2} \exp(-K^2 L^2/2) \left[1 + \frac{4}{Re_t} k^2/K^2 f(\boldsymbol{k}/k,t)\right] \tag{9}$$

where $Re_t = L^2 S/\nu$ is the relevant Reynolds number. Of course the exponent N and the Reynolds number control to what extent the RDT history is affected by viscous decay; inviscid RDT is recovered in the limit of infinite Re_t.

Relationships (8) and (9) will be used for comparing results of viscous RDT with other experimental or numerical results whose initial spectral data are not available. Another application will include an implicit model for decay proposed by Townsend (referred to as RDTT hereafter). This model amounts to specifying in (8) typical values (discussed further) for both Re_t and N ($Re_t = Re^*$ and $N = 4$) assuming an effective viscosity. It is important to point out that the latter model aims at incorporating both viscous effects and *nonlinear transfers* in the dynamics of the largest scales. In that sense, the spectrum model (7) and the universal 'effective' value attributed to $Re^* = L^2 S/\nu_t$ in (9) cannot be considered independently of each other, and cannot be related to 'true' initial data, since they characterize a full – although crude – model for nonlinear interactions. The effective viscosity ν_t was discussed by Townsend (1970, 1976, 1980), Hunt (1978), and Savill (1987). As pointed out by Townsend, a typical value for Re^* ($Re^* = 33.3$) is consistent with the following assumptions: production ($P = -S\langle u_1 u_2\rangle$) and dissipation ($\varepsilon = 5\nu_t q^2/L^2$) of turbulent energy ($q^2/2$) are roughly equal, the ratio ($-\langle u_1 u_2\rangle/q^2$) is nearly constant ($= 0.15$), and the initial transfer of energy between eddies, or ε, is not expected to change greatly during distortion.

3. Two-dimensional energy components

Before computing (§4) 'classic' terms involved in Reynolds stress modelling (RSM) through numerical three-dimensional integration of (8), it is useful to look at quantities

that need only two-dimensional integration and can be obtained analytically. These quantities carry important information about the structure of turbulence, which is not included in the RST.

Following the analysis of streak-like structure in a shear flow without rotation by Lee *et al.* (1990), who compared homogeneous RDT with homogeneous and channel DNS, *two-dimensional energy components* (Cambon 1990)

$$\mathscr{E}_{ij}^{(l)} = \int_0^\infty \langle u_i(\boldsymbol{x},t) u_j(\boldsymbol{x} + r\boldsymbol{s}^{(l)},t)\rangle \mathrm{d}r \tag{10}$$

(with $\boldsymbol{s}^{(l)}$ the unit vector along the direction x_l), are of particular interest, as discussed further in §5. Particularly, the most relevant aspect ratio for elongated structures (denoted 'streamwise eddy elongation parameter' by Lee *et al.* 1990) L^* can be analytically calculated in inviscid RDT as the ratio $\mathscr{E}_{11}^{(1)}/(2\mathscr{E}_{11}^{(3)})$ (Cambon 1990).

The relevance of $\mathscr{E}_{ij}^{(3)}$ was brought to the fore in the case of pure rotation (axis x_3) without mean shear (Cambon & Jacquin 1989; Jacquin *et al.* 1990), as an indicator of the transition from three-dimensional to two-dimensional structure. Since the velocity correlation tensor is averaged onto the direction l, the spatial variability in terms of x_l is removed from consideration, and the contribution from the two-dimensional manifold in planes $x_l =$ constant is displayed. Like the two-point correlation tensor, these quantities are true tensors with respect to the subscripts (i, j) at fixed l. On the other hand, the related integral lengthscales, which are defined by dividing these quantities by the Reynolds stress components, or

$$L_{ij}^l = \mathscr{E}_{ij}^{(l)} / \langle u_i(\boldsymbol{x},t) u_j(\boldsymbol{x},t)\rangle \tag{11}$$

(i, j not summed), have no tensorial properties.

In homogeneous turbulence, the two-dimensional energy components (10) are given by integrating the second-order spectral tensor over the plane $k_l = 0$

$$\mathscr{E}_{ij}^{(l)} = E_{ij}(k_l = 0, t) = \pi \int\int (\Phi_{ij})|_{k_l=0} \mathrm{d}^2\boldsymbol{k}, \tag{12}$$

where $E_{ij}(k_l, t)$ are the so-called one-dimensional spectra, or 'integrated plane spectrum functions' (Batchelor 1953). Clearly, the two-dimensional energy components only involve integration over a plane (a two-dimensional manifold), whereas the Reynolds stress components involve integration over the full three-dimensional wave-space (see (13) below).

Analytical calculations for the case of rotating shear of the integrals in (12), using the RDT relationship (6)–(9) for Φ_{ij}, are given in Appendix B.

3.1. *Spanwise separation*

The related plane $k_3 = 0$ corresponds to the two-dimensional manifold in the plane of the mean flow. When the viscous terms are discarded one easily shows that the spanwise two-dimensional energy components are affected neither by rotation nor by shear, and keep their initial values, where $\mathscr{E}_{11}^{(3)} = \mathscr{E}_{33}^{(3)}/2$ and $\mathscr{E}_{ij}^{(3)} =$ constant. This behaviour is partially recovered (smallest St, highest shear rapidity) in the numerical simulation (DNS) databases by Lee (revisited by Cambon 1990, for computing the two-dimensional energy components) in the case of non-rotating homogeneous turbulent shear flow, but significant viscous and nonlinear effects are exhibited (see figure 2). Hence a refined comparison with DNS results using viscous RDT is given as follows.

Using (9) and (12), the RDT relationships for $\mathscr{E}_{11}^{(3)}$ and $\mathscr{E}_{33}^{(3)}$ display a viscous factor

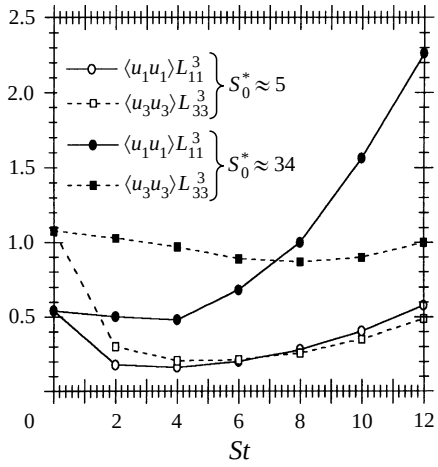

FIGURE 2. Time crossover between the spanwise two-dimensional energy components $\mathscr{E}_{11}^3$ and $\mathscr{E}_{33}^3$, DNS databases of Lee (see Cambon 1990).

which yields a monotonic decrease. This decay is controlled by N ($N > 0$) and the Reynolds number $Re_t = L^2S/\nu$, which can be related to the initial dimensionless shear rapidity: $Re_t = (N+1)S_0^*$, with $S_0^* = (Sq^2/\varepsilon)_{t=0}$.

The decrease of $\mathscr{E}_{ii}^{(3)}, i = 1,2,3$ is shown in figure 3 for $N = 4$ and $S_0^* = 5$ and $S_0^* = 34$, from the Lee database, as in figure 2. In the range $0 \leqslant St < 6$ the viscous RDT results compare with DNS data at high shear rate relatively better than at low shear rate. For $St > 6$ neither viscous RDT nor inviscid RDT can predict the increase in $\mathscr{E}_{11}^3$ in DNS data (especially at high shear rate), indicating increasing effects of the nonlinear straining at large St (ignored in the linear theory). Note that the crossover in the development of $\mathscr{E}_{33}^{(3)}$ and $\mathscr{E}_{11}^{(3)}$, that is observed in DNS at $St \sim 7$ for both high- and low-shear cases (figure 2), could be partially tied to the effects of viscosity, since viscous RDT also yields a crossover, but not at $St = 7$. In short, the linear dynamics of the two-dimensional energy components with spanwise separation is insensitive to rotation, but interesting effects of the shear are taken into account through the viscous RDT term.

3.2. *Streamwise separation*

For $k_1 = 0$ the wave vector is not affected by shear and remains constant $\boldsymbol{k} = \boldsymbol{K}$, so that full analytical solutions can be found for the two-dimensional energy components in the streamwise direction in inviscid or viscous RDT, as shown in Appendix B. In contrast to spanwise two-dimensional energy components, the agreement between DNS results and RDT solutions at $R = 0$ (no rotation) is impressive, as shown in figure 4. Especially, the DNS development at high shear rate is in perfect agreement with the law given by inviscid RDT: $\mathscr{E}_{11}^{(1)}(St)/\mathscr{E}_{11}^{(1)}(0) = 1 + (St)^2/2$.

More generally, these solutions for $\mathscr{E}_{ij}^{(1)}$ are of particular interest since they are sensitive to both shear and rotation, and thus are good candidates for discussing the role of $R = -2\Omega/S$. Inviscid RDT solutions, made non-dimensional by initial values, exhibit the dependence in terms of St and R (B1)–(B4). Viscous RDT solutions are easily derived from inviscid RDT ones by multiplying by a unique factor $(1 + 4\,St/Re_t)^{-N/2}$. Calculations of the same quantities using 'pressureless' approximation (B5)–(B8) exhibit significant differences (with respect to 'exact' RDT), except at $R = 0$, as shown in figure 5. Note that the change of R into $-1 - R$ in the simplified

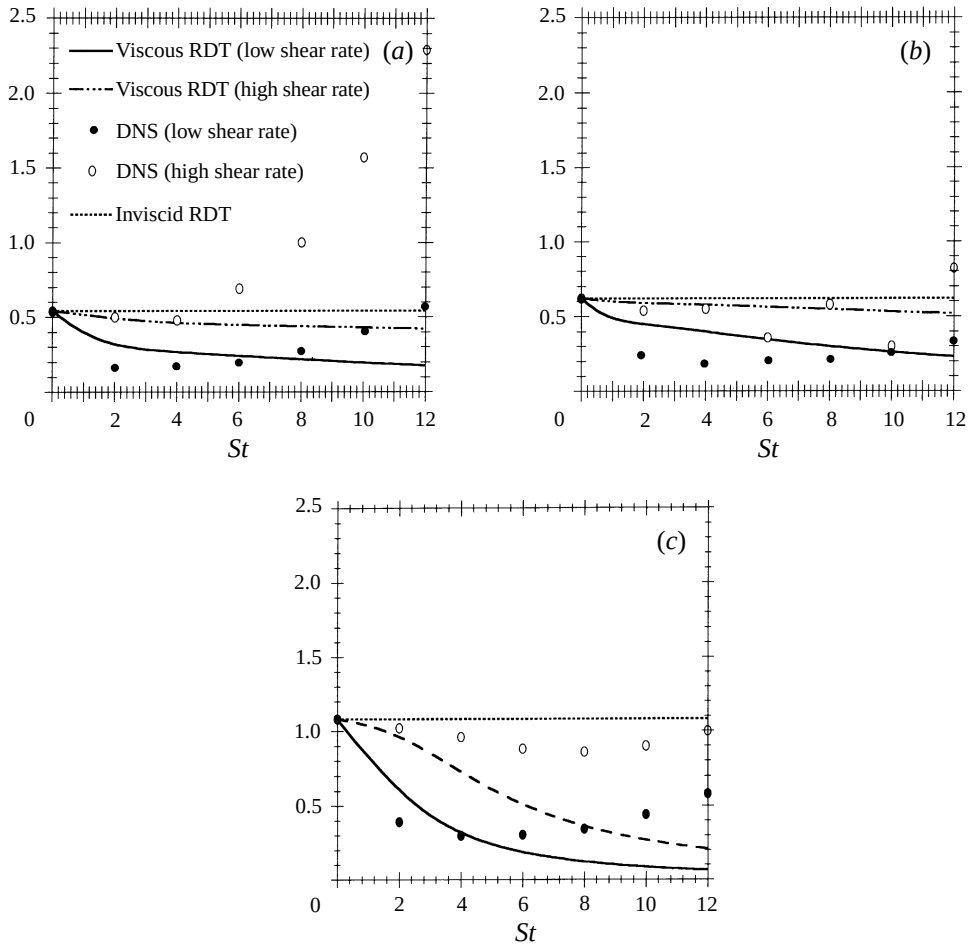

FIGURE 3. Time history of the spanwise two-dimensional energy components: (*a*) $\mathscr{E}^3_{11}$; (*b*) $\mathscr{E}^3_{22}$; (*c*) $\mathscr{E}^3_{33}$. DNS (low shear rate, $S_0^* \approx 5$; high shear rate, $S_0^* \approx 34$). Viscous RDT (low shear rate, $S_0^* = 5, N = 4$ or $Re_t = 25$; high shear rate, $S_0^* = 34, N = 4$ or $Re_t = 170$).

pressureless problem amounts to exchanging the components 1 and 2 (see e.g. (1)), so that only quantities which are symmetric in permuting $(1, 2)$ depend on R through B only, in the pressureless case. This explains why the pressureless distributions in figure 5 are not symmetric with respect to $R \to (-1 - R)$. Hence, effects of pressure are shown in figure 5, but not the effects of pressure on the asymmetry.

4. Comparisons with LES

Since LES data at different R are not available for two-dimensional energy components, only classical single-point correlations are investigated in this section. The Reynolds stress tensor is derived from (6) as

$$\langle u_i u_j \rangle = \int (\Phi^g_{ij}) \frac{E(K,0)}{4\pi K^2} \exp\left(-2\frac{\nu k^2}{S} f(\boldsymbol{k}/k, t)\right) \mathrm{d}^3\boldsymbol{k}. \tag{13}$$

A similar relationship was used by Courseau & Loiseau (1978) in the case of pure shear, with an initial energy spectrum from the experiment of Comte-Bellot & Corrsin

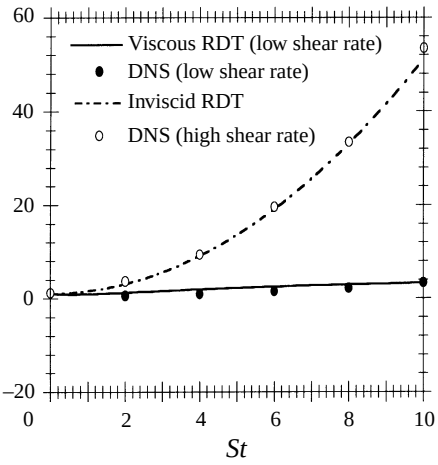

FIGURE 4. Time history of the streamwise two-dimensional energy component $\mathscr{E}^1_{11}$. DNS (low shear rate, $S_0^* \approx 5$; high shear rate, $S_0^* \approx 34$). Viscous RDT (low shear rate, $S_0^* = 5, N = 4$ or $Re_t = 13.5$).

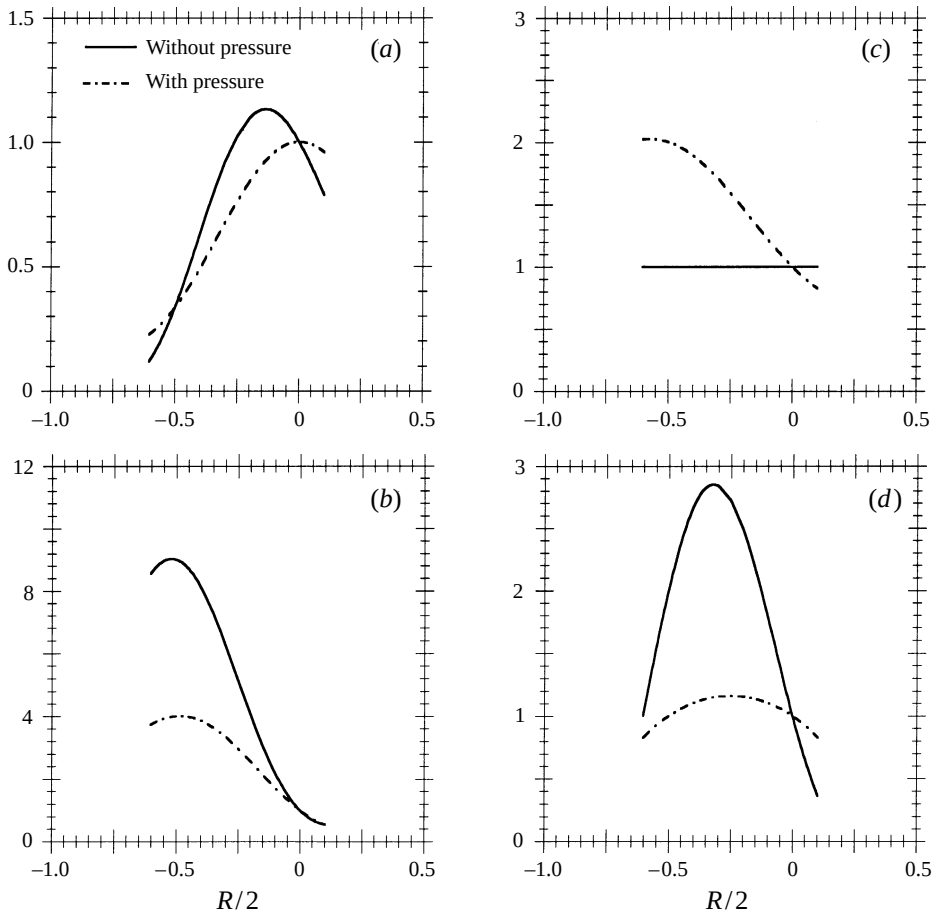

FIGURE 5. Rotation and pressure effects on the streamwise two-dimensional energy components for $St = 2$. (*a*) $\mathscr{E}^1_{11}(R)/\mathscr{E}^1_{11}(R=0)$; (*b*) $\mathscr{E}^1_{22}(R)/\mathscr{E}^1_{22}(R=0)$; (*c*) $\mathscr{E}^1_{33}(R)/\mathscr{E}^1_{33}(R=0)$; (*d*) $\mathscr{E}^1_{12}(R)/\mathscr{E}^1_{12}(R=0)$.

(1971) and a shear rate from the experiment of Rose (1966). The same conditions were used by Bertoglio (1982) for introducing the Coriolis force and performing the first RDT-type computations over the parameter range $-0.824 \leqslant R = -2\Omega/S \leqslant 0.824$. Note that Φ^g_{ij} was derived by the previous authors from the linearized equation for the spectral tensor Φ_{ij} (Craya's 1958 equation), and not from the simpler linear analysis for the velocity fluctuation, so that the link between Φ_{ij} and $\boldsymbol{g}$ was missed. RDTV will denote viscous RDT at the same conditions (initial spectrum, shear rate) as those of Bertoglio.

Using (8) for $E(K,0)$ and $\mathrm{d}^3\boldsymbol{k} = \mathrm{d}^3\boldsymbol{K} = K^2\mathrm{d}K\,\mathrm{d}\theta\mathrm{d}\varphi$, the (13) becomes

$$\langle u_i u_j \rangle = \frac{q_0^2}{8\pi} \int_0^{2\pi} \int_0^{\pi} (\Phi^g_{ij}) \left(1 + \frac{4}{Re_t} \frac{k^2}{K^2} f(\boldsymbol{k}/k, t)\right)^{-(N+1)/2} \sin\theta \mathrm{d}\theta\mathrm{d}\varphi, \tag{14}$$

where $q_0^2/2$ is the turbulent kinetic energy at $t = 0$. For $N = 4$ and $Re_t = Re^* = 33.3$, the expression for the statistical correlations is the same as in Townsend's model introduced in §2.3 and referred to as RDTT.

The only LES results for homogeneous turbulent shear flow in a rotating frame are those of Bardina *et al.* (1983). They used a pseudo-spectral method with a Smagorinsky (1963) model ($C_s = 0.19$); initial data were isotropic, with $2\varepsilon_0/(q_0^2 S) = 0.247$ or, equivalently, a dimensionless shear rapidity $S_0^* = q_0^2 S/\varepsilon_0 = 8.1$ (defined as in §3). (According to Speziale & Mac Giolla Mhuiris (1989*a*), the value $S_0^* = 6.76$ gives better agreement than the former value, and will be used whenever it is necessary.) Note that this initial value of the shear rapidity is very close to the one consistent with the effective Reynolds number in RDTT (using $Re_t = (N+1)S_0^*$ and $N = 4$); this circumstance, which favours the agreement between LES and RDTT results, is fortuitous since Bardina *et al.* (1983) did not use Townsend's arguments (Ferziger, private communication, 1995). The four values of R selected by Bardina *et al.* are the most typical: $R = \infty$ (pure rotation), $R = -1$ (zero absolute vorticity), $R = -1/2$, and $R = 0$.

The results predicted by RDT, RDTV with LES data are compared only for the time history of the turbulent kinetic energy. For the other turbulence statistics such as the Reynolds stress anisotropy tensor, the pressure–strain correlation or the dissipation rate, only the RDTT predictions are compared with LES data. A numerical code is used to derive the matrix $\boldsymbol{g}$ using a fourth-order Runge–Kutta method (analytical solutions for $\boldsymbol{g}$ are obtained for $k_1 = 0, k_3 = 0$, only those needed in §3, and for $B = 0$, see Appendix A). Then the factor Φ^g_{ij} in (14) is constructed by products of $\boldsymbol{g}$ (7).

Only figures in the Bardina *et al.* (1983) report are used for the subsequent comparisons with LES results. The time history of the turbulent kinetic energy for $R = -1, R = -1/2$ and $R = 0$ is shown in figure 6. As in LES, in the different versions of the linear approach the value $R = -1/2$ corresponds to the maximum increase of the turbulent kinetic energy, and there is a difference between the time history of q^2 in the neutral cases ($B = 0$): q^2 increases faster for $R = 0$ than for $R = -1$. For each value of R, the turbulence intensity increases faster when the turbulent Reynolds number (Re_t) increases. It appears that the Townsend model (or RDTT) gives results in fair agreement with LES data, in contrast with present second-order models (see Speziale & Mac Giolla Mhuiris 1989*b*, Salhi, Lili & Sini 1993; Salhi & Lili 1995).

Figure 7 shows the time history of the Reynolds stress anisotropy tensor $b_{ij} = (R_{ij}/q^2 - \delta_{ij}/3)$, exhibiting again a fair agreement between LES and RDTT. Weak discrepancies are found regarding diagonal components, whereas RDTT predicts well the time evolution of the component b_{12}, which accounts for the energy production,

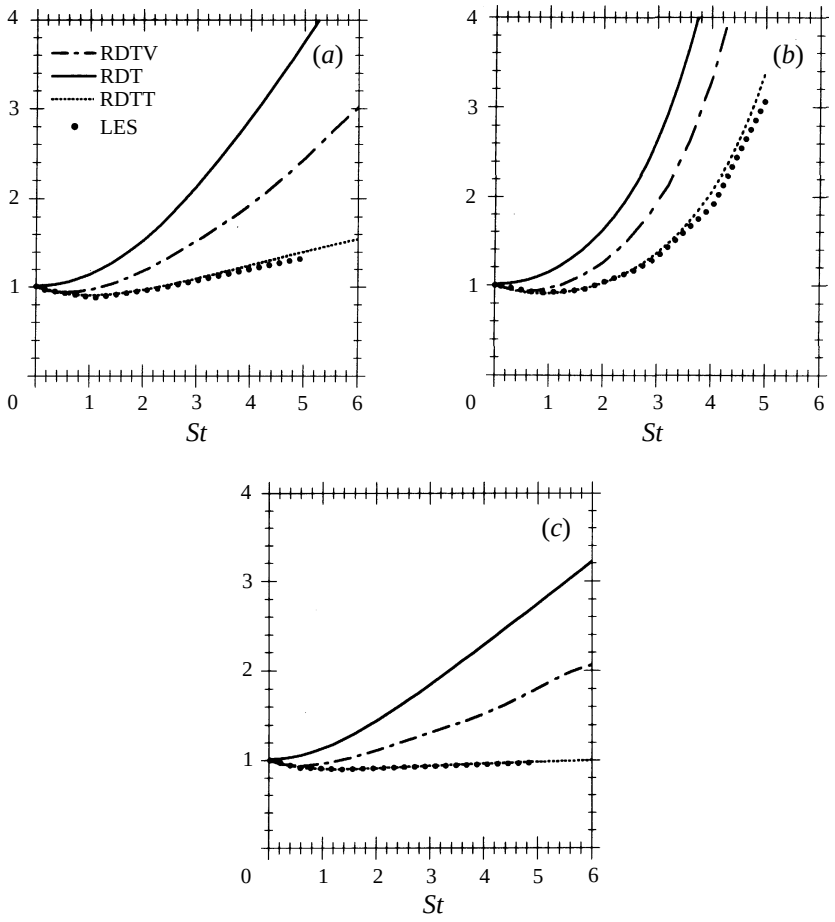

FIGURE 6. Time history of the turbulent kinetic energy non-dimensionalized by the turbulent kinetic energy at $St = 0$. (*a*) $R = 0$; (*b*) $R = -1/2$; (*c*) $R = -1$.

and shows a significant difference between the pure shear flow, $R = 0$, and the zero-absolute-vorticity flow, $R = -1$. In both LES and RDTT, a large decrease (increase in absolute value yielding larger energy production) is observed for $R = -1/2$.

Concerning the RDDT development of the pressure–strain correlation,

$$\phi_{ij} = \left\langle p\left(\frac{\partial u_i}{\partial x_j} + \frac{\partial u_j}{\partial x_j}\right)\right\rangle = \frac{q_0^2}{2\pi} S\left[\delta_{l1}\delta_{m2} + \frac{\Omega}{S}\epsilon_{l3m}\right]$$
$$\int_0^{2\pi}\int_0^{\pi}\left[\frac{k_l k_j}{k^2}(\Phi^g_{im}) + \frac{k_l k_i}{k^2}(\Phi^g_{jm})\right](1 + \frac{4}{Re_t}\frac{k^2}{K^2} f(\boldsymbol{k}/k, t))^{-(N+1)/2}\sin\theta \mathrm{d}\theta\mathrm{d}\varphi,$$

a good agreement with LES is again found, as shown in figure 8 for diagonal components. Note that there is no significant difference between RDTT predictions and LES data for $R = -1$, whereas discrepancies appear for the most destabilizing case ($R = -1/2$).

The dissipation tensor, which is directly obtained in homogeneous turbulence by changing Φ^g_{ij} to $2\nu k^2 \Phi^g_{ij}$ in (13), is now considered. The time history of the dissipation rate $\varepsilon = \varepsilon_{ii}/2$ predicted by RDTT is compared with LES in figure 9. It seems that the linear approach, when compared to LES, takes satisfactorily into account the effect

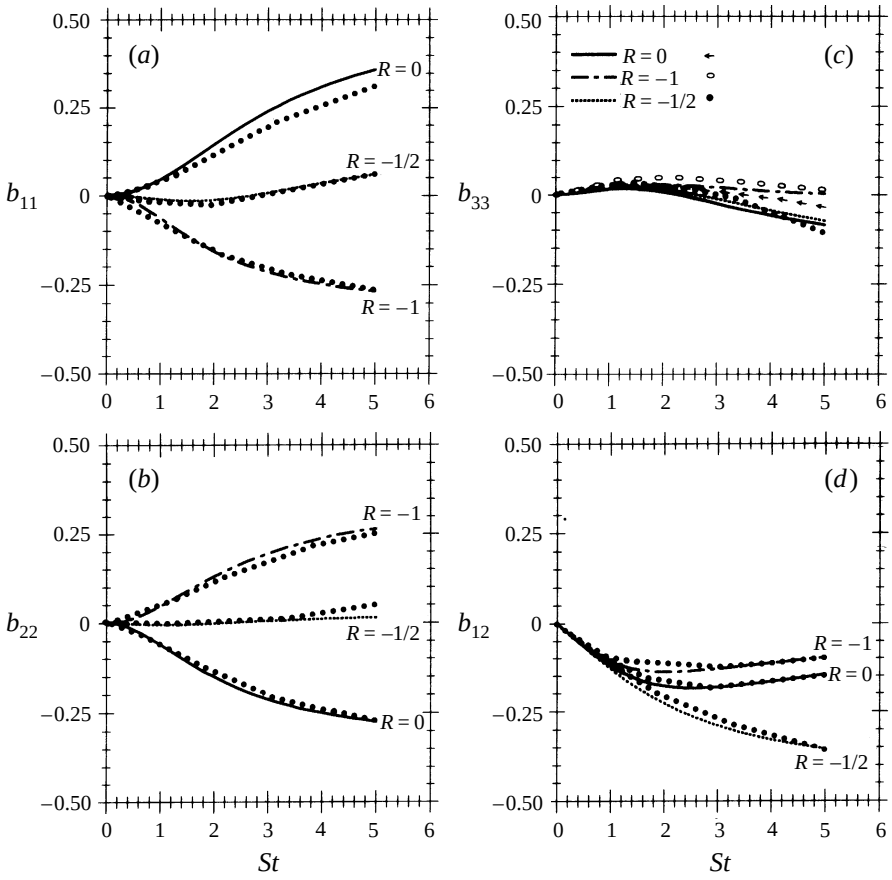

FIGURE 7. Time history of the Reynolds stress anisotropy tensor. Lines, RDTT; symbols, LES. (*a*) b_{11}; (*b*) b_{22}; (*c*) b_{33}; (*d*) b_{12}.

of the rotation number on the dissipation dynamics, even though RDT is expected not to be relevant for the small-scale motions (see e.g. Hunt & Carruthers 1990). One should keep in mind, however, than LES itself cannot predict accurately the small scales which are important for the dissipation spectrum, so that the satisfactory agreement between RDTT and LES has only a relative meaning. Particularly, for $R = -1$ the dissipation rate ε, which is weakly decreasing, is fairly well reproduced by RDTT.

Concerning typical integral length scales, the time history of the streamwise quantity $L_{11}^1 = \mathscr{E}_{11}^{(1)}/\langle u_1^2 \rangle$ is presented in figure 10. The agreement between RDDT and LES is not so satisfactory as previously, even though the DNS history of the related two-dimensional energy component $\mathscr{E}_{11}^{(1)}$ at high shear rate was very well predicted by RDT (figure 4). Unfortunately, it was not possible to extend the RDTT–LES comparisons to all the detailed two-dimensional energy components calculated in §3, since the LES databases (in Bardina *et al.*) were not available, but some qualitative comparisons will be presented in §4.

Finally, the asymmetry with respect to $R = -1/2$ in the development is illustrated in figure 11 by plotting the distribution of statistical quantities (q^2, b_{12}, and b_{33}) as functions of $R, -2 \leqslant R \leqslant 1$ or $-1/4 \leqslant B \leqslant 2$, for a given non-dimensional time

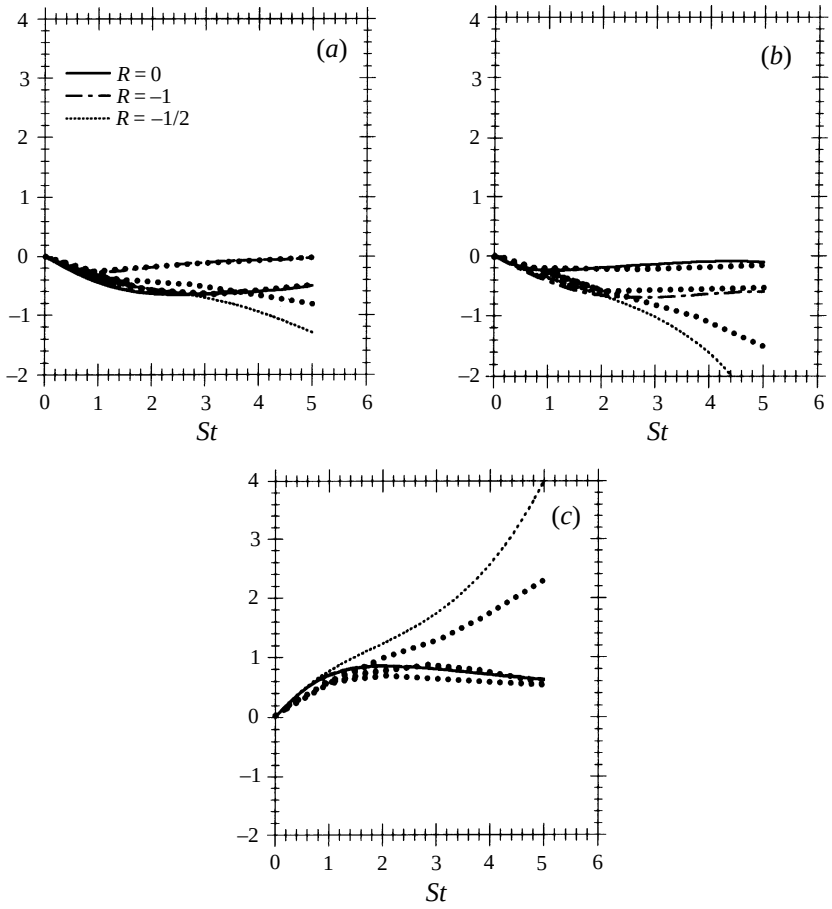

FIGURE 8. Time history of the pressure–strain rate non-dimensionalized by the dissipation rate at $St = 0$; $(\varepsilon/Sq^2)_0 = 0.296$. Lines, RDTT; symbols, LES. (*a*) $\varphi_{11}/2$; (*b*) $\varphi_{22}/2$; (*c*) $\varphi_{33}/2$.

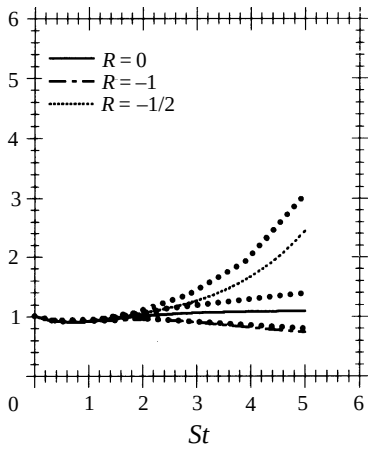

FIGURE 9. Time history of the dissipation rate non-dimensionalized by the dissipation rate at $St = 0$. Lines, RDTT; symbols, LES.

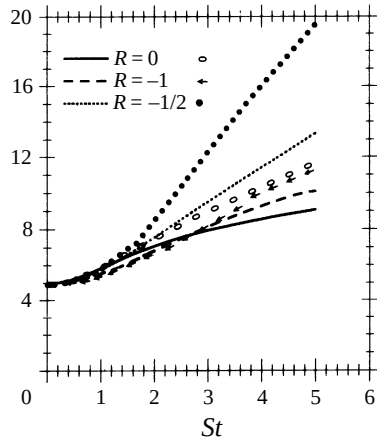

FIGURE 10. Time history of the streamwise length scale, L^1_{11}, non-dimensionalized by the filter width, Δ, used by Bardina *et al.* (1983). Lines, RDTT; symbols, LES.

$St = 5$. This figure indicates clearly that for a given value of B, the rotation has a larger effect on the statistical quantities when R to the left of $R = -1/2$. The maximum magnitudes of q^2 and b_{12} are obtained for $R = -1/2$, and the instability domain predicted by RDT ($-1.2 \leqslant R \leqslant 0.4$ from figure 11*b*) is significantly larger than the one given by $B \leqslant 0$ (or $-1 \leqslant R \leqslant 0$).

5. Towards elongated structures induced by shear in a rotating frame

To characterize the existence of streaky structures in homogeneous turbulence at high shear rate, Lee *et al.* (1990) considered two parameters: 'streamwise energy partition', $W^* = 2\langle u_1^2\rangle/(\langle u_2^2\rangle + \langle u_3^2\rangle)$, and the eddy elongation, $L^* = L^1_{11}/(2L^3_{11}) = \mathscr{E}^{(1)}_{11}/(2\mathscr{E}^{(3)}_{11})$. Their study has shown that the essential mechanism responsible for the appearance of streaks in a wall-layer flow is contained in the linear unbounded theory (homogeneous RDT) at $St \geqslant 8$. Accordingly the threshold values $W^* = 5$ and $L^* = 8$ were proposed to characterize the emergence of streaky structures.

Hence, the relevance of RDT and RDTT with respect to homogeneous DNS is checked, first in the non-rotating case, plotting L^* (figure 12) and W^* (figure 13). RDT, RDTT and DNS results are in excellent agreement for the streamwise partition energy parameter, but not for the eddy elongation parameter at large St from $St = 2$ to 4. The latter unsatisfactory comparison (figure 12) clearly illustrates that some two-dimensional energy components can be more sensitive to subtle nonlinear effects than the quantities obtained by three-dimensional integration over wave-space (such as the Reynolds stress components). Nevertheless, the excellent agreement of DNS with RDT for $\mathscr{E}^{(1)}_{11}$ (figure 4) leads us to distinguish spanwise and streamwise two-dimensional energy components. Clearly, the 'stabilized' growth of L^* found in DNS, which is not reproduced by RDT in figure 12, is essentially due to the underprediction by RDT of the spanwise quantity $\mathscr{E}^{(3)}_{11}$ for $St > 6$ (figure 3*a*) in the ratio $L^* = \mathscr{E}^{(1)}_{11}/(2\mathscr{E}^{(3)}_{11})$.

Regarding the additional effect of system rotation, we can investigate both the homogeneous case and the channel case in a similar way, as Lee *et al.* did (without rotation). It is expected that the results – especially the analytical ones – of §2 and Appendix B will be helpful in explaining the modification or suppression of streaky structures in the vicinity of both the 'pressure-side' and the 'suction-side' walls in

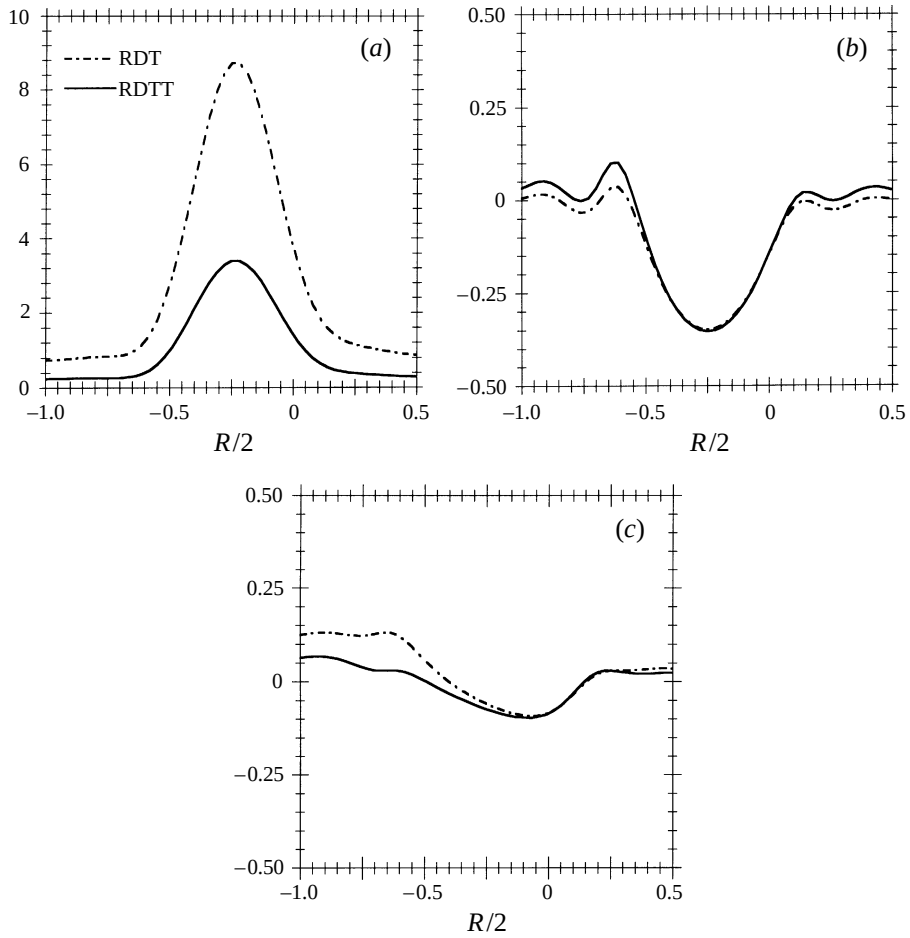

FIGURE 11. Rotation effects on turbulence statistics at $St = 5$. (*a*) $q^2/q^2(0)$ versus R, (*b*) b_{12} versus R, (*c*) b_{33} versus R.

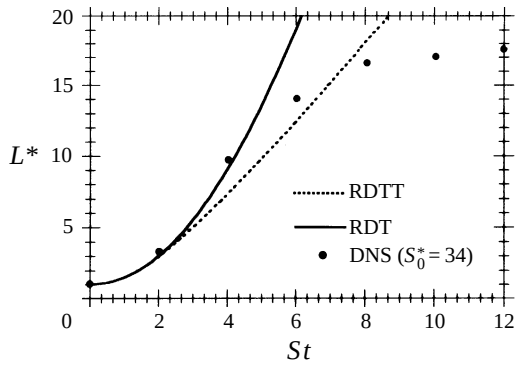

FIGURE 12. Time history of the eddy elongation parameter, L^*, in the pure shear flow case $R = 0$.

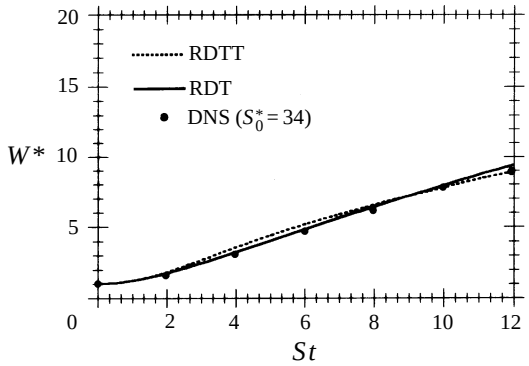

FIGURE 13. Time history of the energy partition parameter, W^*, in the pure shear flow case $R = 0$.

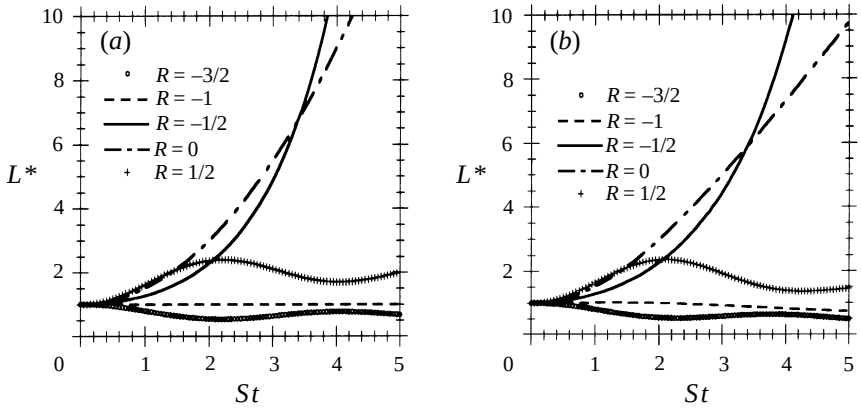

FIGURE 14. Time history of the eddy elongation parameter, L^*, for $R = 1/2,\ R = 0,\ R = -1/2,\ R = -1,\ R = -3/2$. (*a*) RDT, $Re_t = \infty$; (*b*) RDTT, $Re_t = 33.3, N = 4$.

a rotating channel. As has been known for a long time, the pressure-driven side is characterized by a 'destabilization', so that the turbulence is amplified with respect to the non-rotating case, in agreement with $B < 0$. On the same side, the number and intensity of the streaky structures are enhanced, and they also have a strong analogy with the Görtler vortices near a concave wall (Kristoffersen & Andersson 1993). In a large zone around the centreline, a linear mean velocity profile is found, which is in agreement with a zero-absolute-vorticity condition $2\Omega - S = 0$, or equivalently $B = 0$ with $R = -1$; accordingly, the turbulence is found to be not very active in the central region. Near the opposite wall – suction side – the turbulence is stabilized and can completely vanish, in agreement with $B > 0$. Before giving comparisons between DNS results in a rotating channel and the RDT results shown in this paper, figure 14(*a*) presents the development of the quantity $L^* = L_{11}^1/(2L_{11}^3)$ from equations in Appendix B for a wide range of the rotation parameter R, including stabilizing, neutral and destabilizing cases. A strong increase is found for L^* when $R = -1/2$ (the exponential shape of L^* reflects the exponential growth for maximum destabilization) and $R = 0$, (only algebraic growth), whereas L^* remains constant when $R = -1$ (the case of zero absolute vorticity) or oscillates with a weak amplitude when $R = 1/2,\ R = -3/2$ (stable cases $B = 3/4$, see figure 14). The same conclusion can be drawn from the predictions of viscous RDTT (see figure 14*b*).

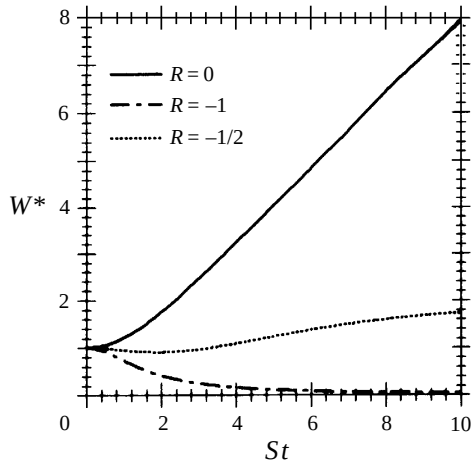

FIGURE 15. Time history of the energy partition parameter, W^*, for $R = 0,\ R = -1/2,\ R = -1$.

From this qualitative analysis, we can infer the following statements.

(i) $L^* \gg 1$ is the only indicator of streamwise elongated structures; it gives the ratio of streamwise to spanwise coherence lengths, independently of the 'jettal' or 'vortical' character of the structures.

(ii) $W^* \gg 1$ is a side indicator, and is of interest only if the structures are jettal; it is relevant in non-rotating shear, where streak-like structures develop with a peak–valley *velocity* distribution (streamwise vorticity is much less relevant than streamwise velocity). On the other hand, only a moderate value ($W^* < 2$) is found for the most destabilizing case (figure 15). This suggest that the elongated structures (identified by high values of L^*) are more vortical than jettal in the case where rotation is destabilizing ($R = -1/2$), in agreement with the fact that these structures resemble co-rotative Görtler vortices near the pressure (destabilized) side of the rotating channel, as mentioned above.

(iii) In the destabilizing case, a 'streamwise vorticity partition' parameter $V^* = \langle\omega_1^2\rangle/(\langle\omega_2^2+\omega_3^2\rangle)$ would be informative, so that $L^* \gg 1$ and $V^* \gg 1$ could characterize elongated vortical structures. The last interesting case is $R = -1$ (zero absolute vorticity). Since $L^* = 1$, the RDT result is consistent with the absence of elongated structures near the centreline of a channel. Nevertheless, the RDT is also consistent with a vortical structure, given by the Cauchy solution of the Helmholtz equation; accordingly, the vorticity parameter V^* is increasing as $(St)^2$ in inviscid RDT at $R = -1$. This increase in V^* is consistent with the decrease in W^* shown in figure 15. As an explanation, one can argue that dominance of the streamwise component of vorticity means dominance of transverse components of velocity, disregarding the difference of scale between velocity and vorticity (smaller scales).

Regarding other possible 'streak detectors' based on statistical quantities, Hunt & Carruthers (1978) pointed out that the RDT development of the energy spectrum $E(k,t)$ for pure shear led to a k^{-2} slope at large times St. Such integer values for the exponent can arise from discontinuities in the velocity field, but can also arise from accumulation points (as explained by Hunt & Vassilicos 1991). k^{-2} slopes were recovered at $R = 0$ in our own calculations, but also for other values (such as $R = -1$) for which no streak-like tendency is observed.

Finally, all the results and inferences of this section suggest (Godeferd 1995) that

the results of homogeneous RDT will compare well with those of DNS-LES in a rotating channel flow *at the same values of* $R = -2\Omega/(\mathrm{d}U_1/\mathrm{d}x_2)$.

6. Summary and conclusions

The case of pure plane shear flow in a rotating frame has been analysed in this paper, with new information gained by means of an extensive RDT approach. This study had three aims:

(i) to estimate, qualitatively and quantitatively, the asymmetry between R and $-1-R$ cases, due to the 'rapid' pressure effect;

(ii) to check the effective viscosity model (RDTT) using available LES data;

(iii) to extend to the rotating cases the 'structural' approach of Lee *et al.* (1990), given the unexpectedly good predictions of homogeneous RDT when compared to DNS in a channel flow without rotation.

Since RDT computations of pure shear flow in a rotating frame are not new, it is necessary to point out two essential characteristics of this work as follows.

First, the starting point is the most general linear analysis, so that linearized equations are those which govern the fluctuating velocity field. The calculation of the matrix $\mathbf{G}$ (equation (4)) gives complete information about stabilization/destabilization, including algebraic as well as exponential growth (as in related studies on hydrodynamic stability, Bayly 1986). In addition, linear solutions for statistical moments of any order, from arbitrary initial data, can be generated using $\mathbf{G}$-products. This generality is lost when solving the 'rapid part' of the equation which governs Φ_{ij} (the so-called Craya equation for the second-order spectral tensor, not recalled here), as previously done by several authors (Deissler 1970; Courseau & Loiseau 1978; Bertoglio 1982).

Secondly, when the total distortion is strong (or $St \gg 1$), analytical solutions are particularly useful. In any numerical method, ranging from integration of RDT equations such as (8) to complete pseudo-spectral DNS, the mean distortion induces a loss of accuracy, which limits the relevance of the computations at $St = 10$ to 15. Even in the 128^3 DNS database from Lee *et al.*, unphysical oscillations are shown in the development of some two-dimensional energy components (see $\mathscr{E}_{22}^{(3)}$ in figure 3*b*), and the relevant range does not exceed $St = 12$.

The results regarding the three aims, quoted above, are as follows

(i) The asymmetry in the development of statistics with respect to $R \to (-1-R)$, due to the 'rapid' pressure effect, has been investigated using RDT in different ways. R-distributions at fixed St are useful provided that only quantities symmetric with respect to $(1,2)$ permutation (e.g. q^2, b_{33}, b_{12}, but not $\mathscr{E}_{ii}^{(1)}$) are considered (see the remark at the end of §3). From this viewpoint the asymmetry shown in figure 11(a,b) at a given St value (=5) is significant but not dramatic. Another way consists of comparing time developments for two cases with the same B-value. As an illustration, the two presumed neutral ($B = 0$) cases $R = 0$ (no rotation) and $R = -1$ (zero absolute vorticity) are found to be completely different from a structural viewpoint: a streak-like tendency develops in the former, but not in the latter, in agreement with the different development of the elongation parameters L^*, W^*, as discussed below.

(ii) Viscous RDT solutions can easily incorporate an effective viscosity model, following Townsend's approach (RDTT), by only specifying the initial energy spectrum and a 'universal' value for the effective Reynolds number. In addition to the (expected) good qualitative agreement between RDT and LES, an excellent quantitative agreement was shown between RDTT and available LES results (Bardina *et*

al. 1983), looking at quantities such as the Reynolds stress components, obtained by three-dimensional integration over wave-space. This strongly suggests that the dynamics of the largest scales is essentially driven by the linear regime. The agreement between RDTT and LES, however, is not so good for quantities such as the spanwise two-dimensional energy components, which involve only the two-dimensional wave-plane normal to the spanwise direction. This confirm that these quantities reflect the nonlinear dynamics in a more explicit and complicated manner than the Reynolds stress components, as previously shown in the case of pure rotation (Jacquin *et al.* 1990; Cambon & Jacquin 1989; Cambon, Mansour & Godeferd 1997).

(iii) An investigation of structure has been performed using RDT, mainly based on the analytical calculations of the spanwise and streamwise two-dimensional energy components in §3. A qualitative analysis has been made with reference to the case of plane channel flow in a rotating frame, in which the range of rotation parameters $R = -2\Omega/(\partial U_1/\partial x_2)$ is very large, when considering different horizontal sections x_2 = constant. It is suggested that the 'streamwise eddy elongation parameter' $L^* = \mathscr{E}_{11}^{(1)}/(2\mathscr{E}_{33}^{(1)})$ only characterizes the tendency to develop elongated structure, and its RDT estimation takes into account the qualitative role of R in a channel flow. The other parameter introduced by Lee *et al.*, 'streamwise energy partition' parameter W^*, is only relevant when the elongated structures are like jets rather than vortices: this concerns the streaks in the non-rotating case, but not the 'reinforced streaks' near the destabilized wall, that seem to be closer to Görtler vortices than to actual streaks. This preliminary work needs to be continued using quantitative comparisons with well-documented DNS data of the rotating channel flow, such as those in Kristoffersen & Andersson (1993).

The authors are grateful to Dr Fabien S. Godeferd and Dr Nicholas Kevlahan for discussions and suggestions. This work was supported by a contract CMCU-95F/1322 for French-Tunisian Academic collaboration

Appendix A. Analytical solutions of the matrix $\boldsymbol{g}$

Several authors (Craya 1958; Herring 1974; Rogallo 1981; Cambon 1982) proposed introducing an orthonormal frame $\boldsymbol{e}^{(1)} = \boldsymbol{n} \times \boldsymbol{k}/ \parallel \boldsymbol{n} \times \boldsymbol{k} \parallel, \boldsymbol{e}^{(2)}, \boldsymbol{e}^{(3)} = \boldsymbol{k}/k$, attached to the wave vector and in which the incompressibility constraint ($k_i \hat{u}_i = 0$) is satisfied by construction, so that

$$\hat{\boldsymbol{u}}(\boldsymbol{k}, t) = \hat{\phi}_1(\boldsymbol{k}, t)\boldsymbol{e}^{(1)}(\boldsymbol{k}) + \hat{\phi}_2(\boldsymbol{k}, t)\boldsymbol{e}^{(2)}(\boldsymbol{k}). \tag{A 1}$$

Here $\boldsymbol{n}$ is a fixed vector, chosen in the vertical direction (figure 1) for obtaining the simplest form of the equations, or $n_i = \delta_{i2}$. The solenoidal modes $\hat{\phi}_\alpha$ (Greek indices take only the value 1 and 2, keeping the summation rule) satisfy an equation similar to (4) (Cambon 1982) as follows:

$$\hat{\phi}_\alpha(\boldsymbol{k}, t) = g_{\alpha\beta}(\boldsymbol{k}/k, t)\hat{\phi}_\beta(\boldsymbol{K}, 0) \exp(-\nu k^2/S) f(\boldsymbol{k}/k, t)). \tag{A 2}$$

The matrix $g_{\alpha\beta}(\boldsymbol{k}/k, t)$ with $g_{\alpha\beta}(t = 0) = \delta_{\alpha\beta}$, unlike the matrix G_{ij} in (4), generates the basic linear solutions with the minimum number of parameters. This matrix $\boldsymbol{g}$ (Cambon 1982; Cambon *et al.* 1994) is close to the matrix denoted $\boldsymbol{A}$ by Townsend (1976) and to the Floquet matrix calculated by Bayly (1986) in the case of the elliptical flow instability. In the case of homogeneous turbulent shear flow in a rotating frame,

the components $g_{\alpha\beta}$ are governed by generic equations

$$\sigma(t)\ddot{y} + \lambda y = 0, \tag{A 3}$$

where $\sigma(t) = K_1^2(St)^2 - 2K_1K_2St + K^2$ and $\lambda = BK_3^2$.

Simple solutions are found when $\lambda = 0$ (i.e. $B = 0, B = \infty$ or $k_3 = 0$) or when $\sigma(t) =$ Constant (i.e. $k_1 = 0$).

For $k_3 = 0$, the transformation matrix is independent of R

$$g_{\alpha\beta} = \begin{pmatrix} 1 & 0 \\ 0 & \dfrac{K}{k} \end{pmatrix}.$$

For $k_1 = 0$, the matrix $\boldsymbol{g}$ has the following form:

$$g_{\alpha\beta} = \begin{pmatrix} \cosh(\omega St) & -(1+R)\dfrac{k_3}{k}\dfrac{\sinh(\omega St)}{\omega} \\ R\dfrac{k_3}{k}\dfrac{\sinh(\omega St)}{\omega} & \cosh(\omega St) \end{pmatrix},$$

where $\omega = (k_3/k)(-B)^{1/2}$. A similar expression is obtained when $B \geqslant 0$.

Townsend (1980) has given the expression for the matrix $\boldsymbol{A}$ in the cases of a simple shear flow, $R = 0$, of a solid body rotation, $R = \infty$ and of an irrotational distortion with axisymmetric, constant circular flow, which is similar to the flow with zero absolute vorticity, $R = -1$. The matrix $\boldsymbol{g}$ has fewer components and simpler forms than the matrix $\boldsymbol{A}$, for instance

$$g_{\alpha\beta}(R = \infty) = \begin{pmatrix} \cos(2\Omega(k_3/k)t) & -\sin(2\Omega(k_3/k)t) \\ \sin(2\Omega(k_3/k)t) & \cos(2\Omega(k_3/k)t) \end{pmatrix},$$

$$g_{\alpha\beta}(R = 0) = \begin{pmatrix} 1 & c \\ 0 & (K/k) \end{pmatrix},$$

$$g_{\alpha\beta}(R = -1) = \begin{pmatrix} 1 & 0 \\ -(k_3/k)St & (K/k) \end{pmatrix},$$

where

$$c = \frac{KK_3}{(K_1^2 + K_3^2)^{1/2}}\frac{1}{K_1}\left[\tan^{-1}\frac{K_2 - K_1St}{(K_1^2 + K_3^2)^{1/2}} - \tan^{-1}\frac{K_2}{(K_1^2 + K_3^2)^{1/2}}\right]$$

in $g_{\alpha\beta}(R = 0)$. Recall that (K_1, K_2, K_3) are the components of the wave vector at $t = 0$.

If we exclude the particular solutions ($k_3 = 0, k_1 = 0$, $R = -1, 0, \infty$) given above, (A 3) can be rewritten as

$$z(1-z)\frac{\mathrm{d}^2y}{\mathrm{d}z^2} - \frac{K_3^2}{K_1^2}By = 0, \tag{A 4}$$

where

$$z = \frac{1}{2}\left(1 - \mathrm{i}\frac{K_2 - K_1St}{(K_1^2 + K_3^2)^{1/2}}\right).$$

Two linearly independent solutions $y_1(z)$ and $y_2(z)$ of (A2) can be found (see Erdeli *et al.* 1953),

$$y_1 = zF(a+1, -a; 2; z),$$

$$y_2 = (1-z)F(-a, a+1; 2; 1-z),$$

where F is the hypergeometric function and

$$a = -\tfrac{1}{2} \quad \text{if} \quad B = K_1^2/(4K_3^2),$$

$$a = -\tfrac{1}{2}(1 \pm [1-(4K_3^2 B/K_1^2)]^{1/2}) \quad \text{if} \quad B < K_1^2/(4K_3^2),$$

$$a = -\tfrac{1}{2}(1 \pm \mathrm{i}[(4K_3^2 B/K_1^2)-1)]^{1/2} \quad \text{if} \quad B > K_1^2/(4K_3^2).$$

As indicated previously, the inviscid linear stability problem is characterized by the matrix $\boldsymbol{g}$. These solutions deserve more attention and will be examined further.

Appendix B. Two-dimensional energy components

Two-dimensional energy components in the streamwise and spanwise directions are derived from the following definitions:

$$\mathscr{E}_{ij}^1 = \langle u_i u_j \rangle L_{ij}^1 = 2\pi \int_0^\infty \int_0^\pi \Phi_{ij}^g(\varphi = \pi/2) \frac{E(K,0)}{4K^2} \exp\left(-2\frac{\nu k^2}{S} f(\boldsymbol{k}/k, t)\right) \mathrm{d}k \mathrm{d}\theta,$$

$$\mathscr{E}_{ij}^3 = \langle u_i u_j \rangle L_{ij}^3 = \pi \int_0^\infty \int_0^{2\pi} \Phi_{ij}^g(\theta = \pi/2) \frac{E(K,0)}{4K^2} \exp\left(-2\frac{\nu k^2}{S} f(\boldsymbol{k}/k, t)\right) \mathrm{d}k \mathrm{d}\varphi.$$

For $k_1 = 0$ and $B \leqslant 0$, the quantities e^g and Z^g in (7) are of the form

$$e^g = 1 + \frac{1}{2}\frac{k_3^2}{k^2}\frac{\sin^2 \omega St}{\omega^2},$$

$$Z^g = -\frac{1+R}{2}\frac{k_3^2}{k^2}\frac{\sin^2 \omega St}{\omega^2} - \mathrm{i}\frac{k_3}{k}\frac{\sin 2\omega St}{2\omega},$$

respectively.

In inviscid RDT ($Re_t = \infty$) one finds

$$\frac{\mathscr{E}_{11}^{(1)}(t)}{\mathscr{E}_{11}^{(1)}(0)} = 1 + \frac{1}{\pi R}\int_0^\pi \sin^2(B^{1/2} St \cos\theta)\mathrm{d}\theta,$$

$$\frac{\mathscr{E}_{22}^{(1)}(t)}{\mathscr{E}_{22}^{(1)}(0)} = 1 - \frac{2}{\pi(1+R)}\int_0^\pi (\cos^2\theta)\sin^2(B^{1/2} St \cos\theta)\mathrm{d}\theta,$$

$$\frac{\mathscr{E}_{33}^{(1)}(t)}{\mathscr{E}_{33}^{(1)}(0)} = 1 - \frac{2}{\pi(1+R)}\int_0^\pi (\sin^2\theta)\sin^2(B^{1/2} St \cos\theta)\mathrm{d}\theta.$$

Similar equations are obtained for $B < 0$. The last integrals are calculated from Gradshteyn & Ryzhik (1965), as follows:

$$\frac{\mathscr{E}_{11}^{(1)}(t)}{\mathscr{E}_{11}^{(1)}(0)} = 1 - \frac{(1+R)}{2}(St)^2\left(-1 + \sum_{j=2}^\infty \frac{(-1)^j (B(St)^2)^{j-1}}{(j!)^2}\right), \tag{B 1}$$

$$\frac{\mathscr{E}_{22}^{(1)}(t)}{\mathscr{E}_{22}^{(1)}(0)} = 1 + \frac{R}{2}(St)^2\left(-\frac{3}{2} + \sum_{j=2}^\infty \frac{(-1)^j (2j+1)(B(St)^2)^{j-1}}{j!(j+1)!}\right), \tag{B 2}$$

$$\frac{\mathscr{E}_{33}^{(1)}(t)}{\mathscr{E}_{33}^{(1)}(0)} = 1 + \frac{R}{2}(St)^2\left(-\frac{1}{2} + \sum_{j=2}^\infty \frac{(-1)^j (B(St)^2)^{j-1}}{j!(j+1)!}\right), \tag{B 3}$$

and

$$\frac{\mathscr{E}_{12}^{(1)}(t)}{\mathscr{E}_{11}^{(1)}(0)} = \frac{-(St)}{2}\left(1 - \frac{B(St)}{2} + \sum_{j=2}^{\infty} \frac{(-1)^j (B(St)^2)^{j-1}}{j!(j+1)!}\right). \tag{B 4}$$

Note that a simpler analytical relationship can be derived when $B^{1/2}St \to \infty$ along the lines of Hanazaki & Hunt (1996). If we consider the spectrum given by equation (8), the behaviours of streamwise two-dimensional components in viscous RDT are related to those obtained in inviscid RDT, as follows:

$$\mathscr{E}_{ij}^{(1)}(t) = \mathscr{E}_{ij}^{(1)}(t, Re_t = \infty)\left(1 + \frac{4(St)}{Re_t}\right)^{-N/2}.$$

When the nonlinear terms and the linear part of the pressure are omitted, for $B \leqslant 0$ the streamwise two-dimensional energy components are (similar expressions are obtained for $B > 0$)

$$\frac{\mathscr{E}_{11}^{(1)}(t)}{\mathscr{E}_{11}^{(1)}(0)} = \cosh^2(-B)^{1/2}St + \frac{(1+R)^2}{2}\frac{\sinh^2((-B)^{1/2}St)}{B}, \tag{B 5}$$

$$\frac{\mathscr{E}_{22}^{(1)}(t)}{\mathscr{E}_{22}^{(1)}(0)} = \cosh^2(-B)^{1/2}St + 2R^2\frac{\sinh^2((-B)^{1/2}St)}{B}, \tag{B 6}$$

$$\frac{\mathscr{E}_{33}^{(1)}(t)}{\mathscr{E}_{33}^{(1)}(0)} = 1, \tag{B 7}$$

$$\frac{\mathscr{E}_{12}^{(1)}(t)}{\mathscr{E}_{11}^{(1)}(0)} = \frac{(R-1)}{4}\frac{\sinh(2(-B)^{1/2}St)}{(-B)^{1/2}}. \tag{B 8}$$

A comparison of these relationship to those given by (B 1)–(B 4) for any value of R shows that the pressure affects the streamwise two-dimensional energy components, except when $R = 0$ (pure shear case) where

$$\frac{\mathscr{E}_{11}^{(1)}(t)}{\mathscr{E}_{11}^{(1)}(0)} = 1 + \frac{(St)^2}{2}, \quad \mathscr{E}_{22}^{(1)}(t) = \mathscr{E}_{22}^{(1)}(0), \quad \mathscr{E}_{33}^{(1)}(t) = \mathscr{E}_{33}^{(1)}(0), \quad \frac{\mathscr{E}_{12}^{(1)}(t)}{\mathscr{E}_{11}^{(1)}(0)} = \frac{-St}{2}.$$

REFERENCES

Bardina, J., Ferziger, J. H. & Reynolds, W. C. 1983 Improved turbulence models based on large-eddy simulation of homogeneous incompressible turbulent flows. *Tech. Rep.* TF–19. Stanford University.

Batchelor, G. K. 1953 *The theory of homogeneous turbulence*. Cambridge University Press.

Bayly, B. J. 1986 Three-dimensional instability of elliptical flow. *Phys. Rev. Lett.* **57**, 2160–2171.

Bertoglio, J. P. 1982 Homogeneous turbulent field within a rotating frame. *AIAA J.* **20**, 1175–1181.

Bradshaw, P. 1969 The analogy between streamline curvature and buoyancy in turbulent shear flow. *J. Fluid Mech.* **36**, 177–191.

Cambon, C. 1982 Etude spectrale d'un champ turbulent incompressible, soumis à des effets couplés de déformation et de rotation, imposés extérieurement. Thèse de Doctorat d'Etat, Université Claude Bernard-Lyon I.

Cambon, C. 1990 Contribution to single and double point modelling of homogeneous turbulence. *Annual Research Briefs*. Center for Turbulence Research, Stanford University.

Cambon, C., Benoit, J. P., Shao, L. & Jacquin, L. 1994 Stability analysis and LES of rotating turbulence with organized eddies. *J. Fluid Mech.* **278**, 175–200.

Cambon, C. & Jacquin, L. 1989 Spectral approach to non-isotropic turbulence subjected to rotation. *J. Fluid Mech.* **202**, 295–317.

Cambon, C., Mansour, N. N. & Godeferd, F. S. 1997 Energy transfer in rotating turbulence. *J. Fluid Mech.* **337**, 303–332.

Comte-Bellot, G. & Corrsin, S. 1971 Simple eulerian time correlation of full and narrow band velocity signals in grid-generated isotropic turbulence. *J. Fluid Mech.* **36**, 273–337.

Courseau, P. A. & Loiseau, M. 1978 Contribution à l'analyse de la turbulence homogène anisotrope. *J. Méc.* **17**, 329–357.

Craya, A. 1958 Contribution à l'analyse de la turbulence associée à des vitesses moyennes. *P.S.T. Ministère de l'air* 345.

Deissler, R. G. 1970 Effect on Initial condition on weak homogeneous turbulence with uniform shear. *Phys. Fluids* **13**, 1968–1969.

Erdeli, A., Magnus, W., Oberhettinger, F. & Tricomi, F. G. 1953 *Higher transcendental functions*, Vols. 1–3. McGraw-Hill.

Godeferd, F. S. 1995 Distorted turbulence submitted to frame rotation: RDT and LES results *Annual Research Briefs*. Center for Turbulence Research, Stanford University.

Gradshteyn, I. S. & Ryzhik, I. M. 1965 *Table of Integrals, Series, and Products*, Vols. 1–3. Academic Press.

Hanazaki, H. & Hunt, J. C. R. 1996 Linear processes in unsteady stably stratified turbulence. *J. Fluid Mech.* **318**, 303–337.

Herring, R. G. 1974 Approach of axisymmetric turbulence to isotropy. *Phys. Fluids* **17**, 859.

Hunt, J. C. R. 1978 A review of the theory of rapidly distorted turbulent flow and its applications. *Fluid Dyn. Trans.* **9**, 121–152.

Hunt, J. C. R. & Carruthers, D. J. 1990 Rapid distortion theory and the 'problems' of turbulence. *J. Fluid Mech.* **212**, 497–532.

Hunt, J. C. R. & Vassilicos, C. 1991 Kolmogorov's contribution to the physical and geometrical understanding of turbulent flows and recent developments. *Proc. R. Soc. Lond.* A, **334**, 183.

Jacquin, L., Leuchter, O., Cambon, C. & Mathieu, J. 1990 Homogeneous turbulence in the presence of rotation. *J. Fluid Mech.* **220**, 1–52.

Johnston, J. P., Halleen, R. M. & Lezius, D. K. 1972 Effects of spanwise rotation on the structure of two-dimensional fully developed turbulent channel flow. *J. Fluid Mech.* **56**, 533–557.

Kristoffersen, R. & Andersson, H. I. 1993 Direct simulations of low-Reynolds number turbulent flow in a rotating channel. *J. Fluid Mech.* **256**, 163–197.

Leblanc, S. & Cambon, C. 1997 On the three-dimensional instabilities of plane flows subjected to Coriolis force. *Phys. Fluids* **9**, 1307–1316.

Lee, J. M., Kim, J. & Moin, P. 1990 Structure of turbulence at high shear rate. *J. Fluid Mech.* **216**, 561–583.

Rogallo, R. S. 1981 Numerical experiments in homogeneous turbulence. *NASA Tech. Mem.* 81315.

Rose, W. G. 1987 Results of an attempt to generate a homogeneous turbulent shear flow. *J. Fluid Mech.* **25**, 97–120.

Salhi, A. 1992 Homogeneous turbulent shear flow in a rotating frame: linear analysis (R.D.T.). *Communication in Euromech 288*. Ecole Centrale de Lyon.

Salhi, A. 1993 Etude des effets de la rotation sur la turbulence, modélisation au second-ordre et analyse linéaire spectrale. Thèse de Doctorat d'Etat, Université Tunis II.

Salhi, A. & Lili, T. 1996 Asymptotic analysis of equilibrium states for rotating shear flows. *Theor. Comput. Fluid Dyn.* **9**, 289–308.

Salhi, A., Lili, T. & Sini, J. F. 1993 An assessment of pressure-strain models for rotating flows. *Phys. Fluids* A **5** 2014–2027.

Savill, A. M. 1987 Recent developments in Rapid Distortion Theory. *Ann. Rev. Fluid Mech.* **19**, 531–575.

Smagorinsky, J. 1963 General circulation experiments with the primitive equations. I. The basic experiments. *Mon. Weath. Rev.* **91**, 99–164.

Speziale, C. G. & Mac Giolla Mhuiris, N. 1989*a* Scaling laws for homogeneous turbulent shear flow in a rotating frame *Phys. Fluids* A **1**, 294–301.

Speziale, C. G. & Mac Giolla Mhuiris, N. 1989*b* On the prediction of equilibrium states in homogeneous turbulence. *J. Fluid Mech.* **209**, 591–615.

STRUBLE, S. A. 1962 *Nonlinear Differential Equations*. McGraw-Hill.

TOWNSEND, A. A. 1970 Entrainment and the structure of turbulent flow. *J. Fluid Mech.* **41**, 13–46.

TOWNSEND, A. A. 1976 *The Structure of Turbulent Shear Flow*, 2nd Edn. Cambridge University Press.

TOWNSEND, A. A. 1980 The response of sheared turbulence to additional distortion. *J. Fluid Mech.* **81**, 171–191.

TRITTON, D. J. 1981 Comments on "Effects of anisotropy and rotation on turbulence production". *Phys. Fluids* A **24**, 1921–1922.

TRITTON, D. J. 1992 Stabilization and destabilization of turbulent shear flow in a rotating fluid. *J. Fluid Mech.* **241**, 1503–523.